JACS
JOURNAL OF THE AMERICAN CHEMICAL SOCIETY

Article

pubs.acs.org/JACS

Proton-Transfer Mediated Enhancement of Nonlocal Electronic Relaxation Processes in X-ray Irradiated Liquid Water

Petr Slavíček,[†] Bernd Winter,[‡] Lorenz S. Cederbaum,[§] and Nikolai V. Kryzhevoi*[,§]

[†]Department of Physical Chemistry, Institute of Chemical Technology, Technická 5, 16628 Prague, Czech Republic

[‡]Joint Laboratory for Ultrafast Dynamics in Solutions and at Interfaces (JULiq), Helmholtz-Zentrum Berlin für Matrialien und Energie, Albert-Einstein-Strasse 15, D-12489 Berlin, Germany

[§]Theoretical Chemistry, Institute of Physical Chemistry, University of Heidelberg, Im Neuenheimer Feld 229, D-69120 Heidelberg, Germany

Supporting Information

ABSTRACT: We have simulated the oxygen 1s Auger-electron spectra of normal and heavy liquid water using *ab initio* and quantum dynamical methods. The computed spectra are analyzed and compared to recently reported experimental data. The electronic relaxation in liquid water exposed to ionizing X-ray radiation is shown to be far more diverse and complex than anticipated and extremely different than for an isolated water molecule. A core-level ionized water molecule in the liquid phase, in addition to a local Auger process, relaxes through nonlocal energy and charge transfer, such as intermolecular Coulombic decay and electron-transfer mediated decay (ETMD). We evaluate the relative efficiencies for these three classes of relaxation processes. The quantitative estimates for the relative efficiencies of different electronic decay modes help determine yields of various reactive species produced by ionizing X-rays. The ETMD processes which are considered here for the first time in the core-level regime are found to have a surprisingly high efficiency. Importantly, we find that all nonlocal electronic relaxation processes are significantly enhanced by ultrafast proton transfer between the core-ionized water and neighboring molecules.

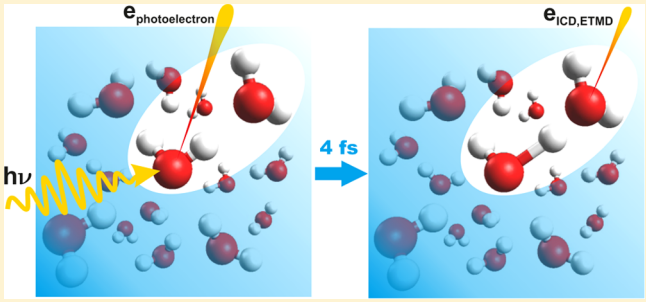

INTRODUCTION

Core-level ionization of water is followed by a plethora of relaxation processes involving both nuclear and electronic dynamics and can lead to X-ray fluorescence, nonadiabatic transitions, dissociation, molecular rearrangement, or Auger-electron decay.[1,2] Understanding these processes in water, which is the main component in biological cells, is of fundamental importance. Also, the damage of biological tissues by radiation is supposed to be caused primarily by the interaction with products of water radiolysis rather than by direct ionization of biomolecules.[3] Yet the nature and character of reactive intermediates remains elusive.

The major initial relaxation pathway upon core-level ionization of water in the gas phase is the (local) Auger decay. In this process, the created core hole is refilled by a valence electron, and the released energy is used to ionize another valence electron from the same water molecule. In core-ionized liquid water, nonlocal electronic decay routes also become possible. One process resembles intermolecular Coulombic decay (ICD)[4] where the created hole is still refilled by a valence electron from the same site, but the secondary electron is now emitted from a neighboring molecule. This leads to a situation where the two charges are spatially separated, and two neighboring ions are produced.[5−10] These electrons have been associated with the high kinetic energy shoulder characteristic of the Auger spectra from liquid water and large water clusters.[6] Here, we show that another, yet unconsidered, mechanism resembling electron-transfer mediated decay (ETMD)[11] also contributes to the high kinetic energy electron intensity. Both ICD and ETMD have been originally theoretically predicted to occur after inner-valence ionization[4,11,12] (see also the recent reviews of theoretical and experimental work on ICD and related phenomena).[13,14] So far ETMD has been confirmed experimentally only for this energy regime.[15,16] Unlike for Auger decay and ICD, the created core hole in an ETMD process is refilled by an electron from a neighboring molecule, thus neutralizing the initially ionized molecule and subsequently ejecting another electron from this neighboring molecule. This is the so-called ETMD(2) process. If the hole refill is by a valence electron from another neighboring water molecule, the process is referred to as ETMD(3). An illustration of the Auger decay and the nonlocal core-level ICD-like and ETMD-like processes (thereafter denoted ICD and ETMD for convenience, respectively) is shown in Figure 1.

Since the lifetimes of core-level vacancies are extremely short, on the order of few femtoseconds, the whole sequence of

Received: November 15, 2014
Published: December 10, 2014

   dx.doi.org/10.1021/ja5117588 | J. Am. Chem. Soc. 2014, 136, 18170−18176

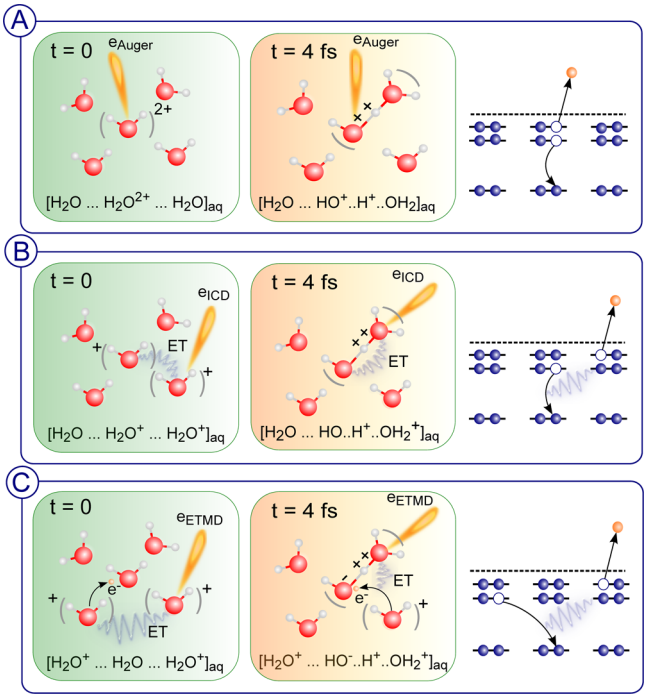

Figure 1. Schematic representation of the local Auger-electron decay (panel A) and the nonlocal ICD (panel B) and ETMD (panel C) processes in liquid water after core ionization. In the first column, the electronic relaxation processes are presented for the ground-state geometry of the model water pentamer. In the second column, the same processes are shown for geometries resulting from PTM-CS. The molecular species involved in the respective electronic decay are enclosed in brackets, and their final ionic states are indicated. ET denotes energy transfer. Electronic levels and the respective electron transitions are shown in the third column.

ionization and subsequent electronic relaxation is commonly considered a vertical process, i.e., it does not include nuclear motion. The vertical character of the autoionization transitions is, however, disputable for hydrogen-bonded systems. Here, a light proton can move a significant distance, even within the short time needed to refill the core hole by another electron. This has been demonstrated in several studies using X-ray emission and resonant Auger-electron spectroscopies.[17−25]

Very recently, unambiguous experimental evidence for ultrafast proton-transfer dynamics following core-level ionization of liquid water has been provided based on O 1s Auger-electron spectra of normal liquid water, H_2O, and its deuterated analogue, D_2O, using the technique of liquid microjets.[26] The analysis of the experimental spectra, based on quantum chemical calculations, revealed a novel type of relaxation processes, termed proton-transfer mediated charge separation (PTM-CS; also shown in Figure 1). In this process, the autoionization occurs after a proton has moved away from the core-ionized water unit toward a neighboring hydrogen-bond (H-bond) acceptor water molecule (a proton-transferred geometry). In the PTM-Auger process, the emerging intermediate core-ionized Zundel-like cationic structure, $OH^*\cdots H^+\cdots H_2O$, is transformed into a charge-separated $OH^+\cdots H_3O^+$ complex.

The explanation of the distinct Auger-electron spectra of normal and heavy liquid water invoking the PTM-CS mechanism[26] has provided deeper understanding of the dynamics of X-ray irradiated liquid water. The remaining question of major importance concerns the impeccable identification of all the potential electron relaxation mechanisms and their efficiencies. This issue is of great practical importance, for instance, when attempting to identify and quantify various genotoxic species formed upon X-ray ionization. However, kinetic energies of the electrons emitted in different relaxation processes are similar. For example, electrons due to the ICD and PTM-Auger contribute mainly to the high kinetic energy shoulder in the Auger spectrum, making their distinction and thus their relative importance elusive, at least when based on the current experimental data alone. Here, we need to invoke theoretical calculations for interpreting the measured autoionization spectra.

METHODS

Experimental Section. Photoelectron spectroscopy measurements were performed from a 15 μm vacuum liquid water jet at the soft-X-ray U41-PGM undulator beamline ($\approx 23 \times 12$ μm^2 focal size) of BESSY II, Berlin. The jet velocity was approximately 80 $m \cdot s^{-1}$, and the jet temperature was 6 °C. Under these conditions, the pressure in the vacuum chamber is typically 1×10^{-5} mbar. Electrons were detected with a hemispherical electron analyzer, separated from the liquid jet by a 100 μm diameter orifice at a distance of approximately 300 μm. Detection angle was normal with respect to the light polarization vector in order to minimize photoelectron contributions from the direct ionization of the O 1s orbital of water. Energy resolution of the 600 eV X-rays used here was approximately 150 meV, and the energy resolution of the electron analyzer was better than 200 meV. Highly demineralized (0.2 μS/cm) water, H_2O, and D_2O was used for the liquid jet, and small amount of NaCl has been added (0.02 M concentration) to compensate for electrokinetic effects and charging upon photoionization. The experimental spectra have been already published in ref 26 and are shown here for comparison with the theoretical results only. A more detailed description of the experiment can be found in ref 27.

Computational. In our calculations, we separate nuclear and electronic motions. We consider the motion of a proton along a proton-transfer coordinate as the main dynamical process occurring on the short lifetime of the O 1s core hole. The choice of this coordinate is discussed in more detail in the Supporting Information. The propagation of the wavepacket describing proton motion from the central water unit to an H-bond acceptor water molecule was simulated using quantum dynamical calculations. The static Auger spectra were computed separately for selected grid points along the proton-transfer coordinate. Finally, we convoluted the computed nuclear densities with the static Auger spectra to obtain time-dependent dynamical Auger spectra.

The Wavepacket Dynamics. The wavepacket-dynamics calculations were performed on the CASSCF potential energy surface with frozen core orbital occupations. Only the orbitals occupied in the ground state have been included into the active space (consisting of 49 electrons in 25 orbitals). The aug-cc-pCVDZ basis was used for oxygen and the aug-cc-pVDZ basis for hydrogen atom.[28,29] The nuclear wave function was propagated on the core-ionized potential energy surface using a split operator technique. The wavepacket was discretized on 1024 grid points on a grid ranging from 0.6 to 2.2 Å. A time step of 1 au was used in the propagation. The initial wave function was obtained by wavepacket propagation in the imaginary time on the ground-state potential energy surface calculated at the Hartree−Fock level. The electronic structure calculations were done with MOLPRO suite of codes.[30]

Calculations of the Auger-Electron Spectra. The kinetic energies of the electrons emitted in the core-hole decay were obtained by subtracting valence double ionization potentials (DIPs) from the single ionization potentials of core electrons. The latter were obtained using the CASSCF method as described above. The DIPs were computed using the second-order algebraic diagrammatic construction (ADC(2)) method, which is an approximation scheme for the two-particle propagator.[31,32] Here, a relativistic pseudopotential basis set[33]

dx.doi.org/10.1021/ja5117588 | J. Am. Chem. Soc. 2014, 136, 18170−18176

augmented with one s-type diffuse and one polarization d-type function was used for oxygen atoms and the cc-pVDZ basis set[29] for hydrogens.

The ADC(2) method also yields the transition moments between the ground state and the dicationic states. A two-hole population analysis[34] enables us to partition these transition moments into various contributions distinguished by different localizations of the final valence holes and consequently to determine the character of each dicationic state. We can distinguish between the Auger (two holes are localized on the central molecule), the ETMD(2) (two holes residing on a peripheral molecule), the ICD and ETMD(3) contributions (two holes are distributed between two different molecules). The ICD and ETMD parts can further be decomposed into contributions due to the H-bond donor and H-bond acceptor water molecules. The Auger contributions are used as intensities of the spectral lines. Each spectral line is finally convoluted with a Gaussian with fwhm = 3.0 eV. Using this procedure, a manifold of the static Auger spectra $\tilde{\sigma}(E_{kin}; x_i)$ was produced for the grid points along the proton-transfer coordinate changing from 0.75 to 1.90 Å, with the step 0.05 Å. E_{kin} is the kinetic energy of the emitted electrons.

The effects of nuclear density distribution and time evolution were incorporated to the Auger spectra as follows. The nuclear densities $|\psi(x; t_n)|^2$ computed for the different times t_n were split into vertical stripes centered on the grid points x_i, and the areas of these stripes, $a(x_i; t_n)$, were found. The static Auger spectra $\tilde{\sigma}(E_{kin}; x_i)$ were then multiplied by the coefficients $a(x_i; t_n)$, and the products were summed up. Accounting for the electronic decay, the norm of the wavepacket is taken to decrease exponentially as e^{-t/τ_c}, where τ_c = 3.6 fs is the core-hole lifetime, the Auger spectral distribution formed during a time interval $\Delta t = t_n - t_{n-1}$ can be expressed as

$$\sigma(E_{kin}; t_n) = (e^{-t_{n-1}/\tau_c} - e^{-t_n/\tau_c}) \sum a(x_i; t_{n-1})\tilde{\sigma}(E_{kin}; x_i)$$

RESULTS AND DISCUSSION

As a model system for our calculations, we consider a water pentamer in a distorted tetrahedral geometry. The tetrahedral coordination accounts well for the hydration structure arrangement and the specific H-bond interactions in ice. The tetrahedral arrangement of the first solvation shell pertains according to the standard view even in liquid water;[35] this assumption is however a subject of ongoing debate.[36−41] We then focus on the core-level ionization of the central, fully solvated water unit. The distances from this molecule to peripheral ones were set at 2.8 Å[35] to account for shorter O···O distances in liquid water as compared to free water clusters. We have also explored the sensitivity of the calculated quantities to the particular geometries by considering water pentamers with the O···O distances of 2.74 Å (found in I*h* ice), 2.70 and 2.90 Å (see the Supporting Information). Because of the short times involved in the processes studied here, we keep in our simulations all atom positions fixed, except for that of a single proton of the central monomer (the one being ionized) which can move toward a neighboring water molecule as mentioned above. A core-ionized water molecule in liquid can in fact lose both protons. The transfer of the second proton starts, however, at a much later time than the transfer of the first one [21] and is thus not expected to significantly affect the Auger electron spectra. The presence of hydrating water molecules in both the H-bond donor and acceptor positions relative to the central water monomer allows for the systematic investigation of the different effects of these molecules on the relaxation dynamics which is difficult to obtain from the experiment. We stress that in contrast to a water dimer which is often used as a model system for liquid water, the pentamer does support ETMD(3) processes. These play indeed a surprisingly important role in the overall relaxation dynamics as will be shown below. We compute the Auger-electron spectra of both the normal and heavy water pentamers, as described in the Computational methods section, and compare with experiment.

Theoretical prediction of the time evolution of the Auger-electron spectrum of the normal (light) water pentamer including nuclear motion of the proton is presented in Figure 2 for the spectral region involving outer-valence electron

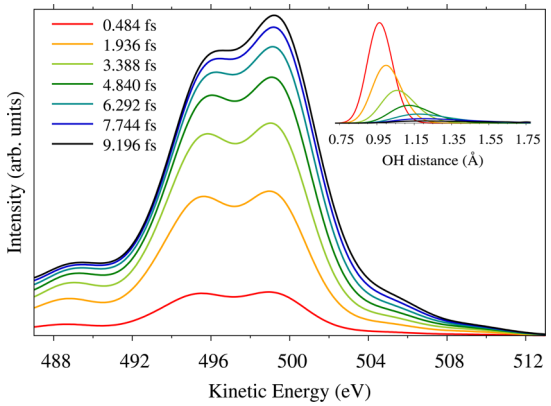

Figure 2. Theoretical simulations of the time evolution of the Auger-electron spectrum of the central molecule in the normal (light) water pentamer. Ultrafast proton motion accompanying electronic relaxation is taken into account, leading to considerable changes of the spectral shape, especially in the high kinetic energy part, above 501 eV. The proton motion is described by the propagation of the wavepacket on the core-ionized potential. The variations in shape and in position of the wavepacket with time are shown in the inset. The norm of the wavepacket in the inset decreases exponentially with a time constant of 3.6 fs to account for the changing population in the core-ionized state.

transitions (i.e., the leading Auger spectrum). The lowest curve relates to the electronic and nuclear relaxation processes in the early time after ionization, i.e., when the dominant contribution to the spectrum is associated with the ground-state geometry. In the spectrum, one observes two main peaks which are attributed to the local Auger decay. These spectral features move toward approximately 1 eV higher kinetic energies when the decay is completed. Their intensities increase by different amounts, and the peak near 499 eV becomes more pronounced when the decay is complete. Besides the two main peaks, one also observes a small bump in the low kinetic energy region, at around 488.5 eV, which is mainly due to the local Auger decay, producing two holes in the $1b_2$ orbital of the core-ionized monomer, but nonlocal processes contribute here as well. The most striking spectral feature is however the shoulder at the high kinetic energy side, at around 507 eV. It is essentially absent at very early times, quickly acquiring intensity within a few femtoseconds. Apparently, the temporally evolving large spectral changes, and especially the ones at high kinetic energy, result from the ultrafast proton motion accompanying electronic relaxation.

Experimentally, nuclear dynamics are tracked via isotopically substituted water, namely by comparing the Auger-electron spectra measured for liquid H_2O and D_2O. Such a measurement has been recently performed,[26] and the corresponding experimental spectra are reproduced in Figure 3. The figure also shows the theoretical Auger spectra with the intensities accumulated up to the time instants ∼0.5 and ∼9.7 fs. It is seen that the experimental Auger spectra (top tier) are significantly

dx.doi.org/10.1021/ja5117588 | J. Am. Chem. Soc. 2014, 136, 18170−18176

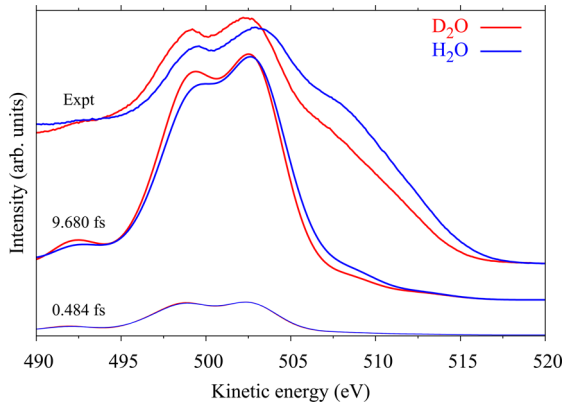

Figure 3. Comparison of the experimental spectra from light and heavy liquid water (top tier) with the theoretical Auger spectra of the light and heavy water pentamers. Photon energy was 600 eV. The simulated spectra are shown for two time instants: ~0.5 and ~9.7 fs (bottom and central tiers, respectively), corresponding to the initial and final phases of the electronic decay. In the former case, the spectra of the normal and deuterated pentamers are almost indistinguishable. The theoretical spectra are shifted to larger energies by 3.4 eV to account for long-range polarization effects which are apparently missing in our finite size system. The somewhat smaller broadening of the calculated spectra is due to the single pentameric structure used in our calculations which cannot represent the rich hydration structure variations characteristic of liquid water. Furthermore, in our calculations all other coordinates are frozen which also has an effect on the simulated spectra.

different for normal and deuterated liquid water. The high kinetic energy shoulder is considerably weaker in deuterated water. This is consistent with the proton-transfer mediated enhancement of the process leading to the high kinetic energy electrons. Indeed, a proton is able to move faster than a deuteron, and the wavepacket may propagate further on the core-ionized state before it decays completely. This trend is well reproduced by our calculations. In the center tier of Figure 3, the theoretical Auger-electron spectra are shown for the normal and heavy water pentamers when the electronic relaxation of the core-ionized state is essentially complete. The difference between these spectra closely resembles the experimentally measured one, both in the central spectral region and for the high kinetic energy shoulder. The latter is more enhanced for the normal water pentamer. Such a large isotope effect cannot be assigned to the difference in the ground-state vibrational wave functions of the two isotopologues. If this were true, the computed spectra should already differ in the initial phase of the relaxation process. However, as one can see from the bottom tier of Figure 3, the corresponding Auger spectra of $(H_2O)_5$ and $(D_2O)_5$ are almost identical.

Comparison of the Auger-electron spectra of normal and heavy water reveals that the autoionization processes are indeed controlled by the degree of proton transfer among the adjacent water units. However, the experimental spectra alone provide rather limited insight into the type of the relaxation processes contributing to the spectrum, and no information on their relative efficiencies can be inferred. Also, temporal evolution of these processes cannot be extracted from static experimental spectra. Therefore, electronic structure calculations have been carried out to disentangle the nature of the electronic relaxation processes. In contrast to Figures 2 and 3, showing the Auger spectra computed dynamically up to the given time evolutions and thus including contributions from all cluster geometries, Figure 4 shows the Auger spectra (black curves) calculated at three different representative geometries of the normal water

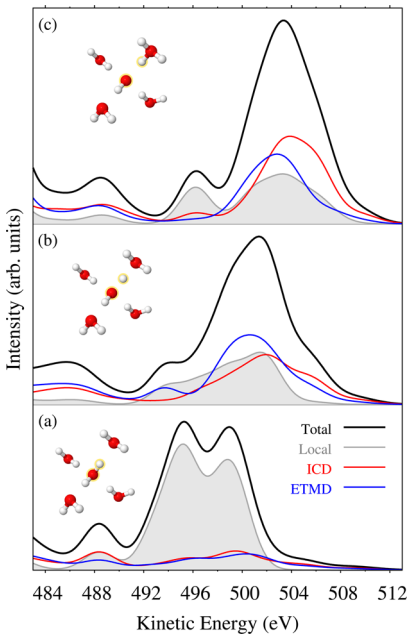

Figure 4. Simulated Auger-electron spectra (thick black curves) for three different geometries of the water pentamer (shown in the insets) with the proton-transfer coordinates (a) 0.95 Å (the ground-state geometry), (b) 1.40 Å (a Zundel-like structure), and (c) 1.85 Å (water−hydronium complex). The areas under the gray (shaded area), red, and blue curves reflect the contributions of the Auger, ICD, and ETMD processes, respectively, to the total spectral intensity.

pentamer along the proton-transfer coordinate. Spectral contributions from different electronic relaxation pathways are shown as well.

The spectrum corresponding to the ground-state geometry (Figure 4a) is mainly associated with the local Auger processes (see the gray shaded area), except for the rather weak high kinetic energy part (>503 eV) resulting exclusively from the nonlocal ICD and ETMD processes (red and blue curves, respectively). This spectrum and those shown in Figures 2 and 3 for early times of the electronic decay are seemingly similar.

The Auger spectrum computed for the cluster with a proton located exactly halfway between two water molecules, i.e., for the Zundel-like structure forming in PTM-CS processes, is shown in Figure 4b. Several observations can be made here. First, compared to Figure 4a, the whole spectrum is shifted toward higher kinetic energies of the emitted electrons. Thereby the local Auger states experience a particularly strong energy shift. This is caused by the fact that the final charge-separated states $OH^+\cdots H^+\cdots H_2O$ populated in the Zundel-like moiety via Auger decay have significantly lower energies than the final one-site Auger states $H_2O^{2+}\cdots H_2O$ available in the cluster at the ground-state geometry. This effect is further enhanced in the data shown in Figure 4c for the pentamer with the O−H distance set to 1.85 Å which corresponds to the formation of a hydronium molecule.

The above-discussed energy shift in the spectra of Figure 4 is however not the only effect. We also observe a strong change in the spectral shape in response to deprotonation of the central water molecule. In particular, the double-peak structure (Figure 4a) turns into a single asymmetric peak as seen in Figure 4b,c.

dx.doi.org/10.1021/ja5117588 | J. Am. Chem. Soc. 2014, 136, 18170−18176

Because of this shoveling of intensity, the major peak at ∼499 eV in the time-resolved spectra (Figure 2) gains more intensity than the others, as time evolves.

Large variations of the spectral contributions of the different relaxation processes are also seen in Figure 4. The most important observation is that at the proton-transferred geometries, the local decay mode is no longer dominant, and the nonlocal ICD and ETMD processes play a pivotal role. The remarkable enhancement of the nonlocal modes has different origins depending on the spectral regions considered. In the middle part of the spectrum, <503 eV, the final ICD and ETMD states overlap well in energy with the final Auger states. Because of this near-degeneracy, all states interact and mix strongly with each other causing substantial intensity redistribution from the Auger states to the ICD and ETMD ones. Recently, this effect has been demonstrated to lead to a 10-fold enhancement of the ICD efficiency in ammonia clusters.[10] In the outermost high kinetic energy part of the spectrum, >503 eV, where the local and nonlocal final states hardly overlap energetically, the intensity gain of the latter is a consequence of hybridization and thus of a better spatial overlap of the molecular orbitals[45] in proton-transferred complexes relative to those in the cluster with the ground-state geometry.

We next comment on the surprisingly large contribution due to ETMD, which was expected to be inefficient in competing with Auger or ICD decay. For rare-gas clusters this is indeed the case.[11] In contrast to water pentamer considered here though these clusters are characterized by large interatomic distances, and their orbitals are highly localized on different centers, and thus overlap only slightly with each other. That is, any prerequisites for efficient charge transfer are absent. We note that in the water pentamer, ETMD(3) plays a more important role than ETMD(2), as can be inferred from Figure 4 when comparing the peak areas. The peaks in the ETMD curve at 495 eV in Figure 4a and at 493 eV in Figure 4b are the only structures due to ETMD(2). As one can see, the importance of ETMD(2) changes only marginally, while that of ETMD(3) increases dramatically with proton motion. This can be explained by the energy overlaps between the corresponding ETMD states and the Auger ones: the energy overlap between the ETMD(2) and Auger states weakens, while that between the ETMD(3) and Auger states gets stronger when a proton moves. Thus, instead of being localized on a single water monomer neighboring the initially core-ionized water molecule, the two final outer-valence vacancies formed in ETMD tend to delocalize into the environment.

Interestingly, in the earlier stages of the electronic and nuclear relaxation, ETMD(3) mainly affects the H-bond donor water molecules, making them cationic. Upon proton transfer and ensuing charge separation, the energies of these particular ETMD(3) states do not change much. In contrast, the energies of the Auger states change substantially and so do the energies of those ETMD(3) states where one vacancy is created on the water molecule accepting the proton while the other one forms on either of the H-bond donor water molecules. As a consequence, the above Auger and ETMD(3) states start to interact strongly and the ETMD(3) efficiency increases. A similar trend is observed in the ICD processes with the only difference that one of the vacancies is always created on the initially ionized central water molecule. This is depicted in Figure 1.

Figure 5 shows the populations of the Auger, ICD, and ETMD final states for the whole spectral region at different

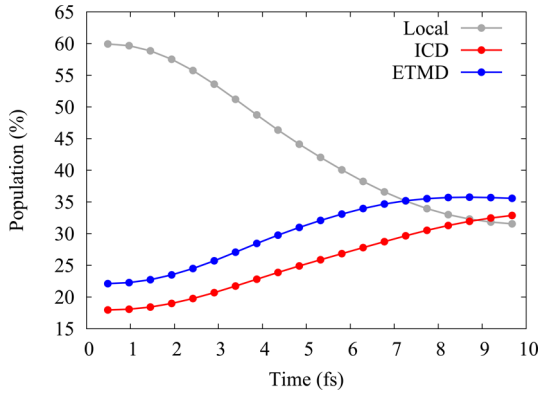

Figure 5. Populations of the final states by different competing electronic relaxation processes in the model water pentamer computed for different time instants.

time instants, *t*. These were obtained by determining the areas of the respective contributions to the total spectral intensities of the dynamical Auger-electron spectra. These populations can be considered as measures of the efficiencies of the corresponding processes. At shorter times, the local Auger processes prevail, although their dominance is not as pronounced as one might expect. Indeed, nearly 40% of all final states are of nonlocal character, i.e., they are populated via ICD and ETMD. Many such states are found at energies corresponding to the center part of the spectrum and are thus difficult to identify experimentally. The relative efficiency of the nonlocal processes increases strongly for later times, accounting for ∼70% of the population at t = 10 fs. As for the high kinetic energy spectral part alone (above 501 eV in Figure 2), here, we find that the contribution of the nonlocal decay modes constitutes about 75%. This fraction changes little with time.

In liquid water, the nonlocal processes are expected to be more efficient than in the model water pentamer because of a larger number of molecules participating in ICD and ETMD. The effect of cluster size on electronic decay is demonstrated in Figure S1 of the Supporting Information, comparing the computed Auger spectra of a water pentamer and a trimer (a trimer is chosen as the smallest system where ETMD(3) processes are possible). As one can see, besides the noticeable intensity enhancement of the high kinetic energy shoulder in the Auger spectrum with growing cluster size, there is also a remarkable change in the relative significance of the different relaxation modes. We also note that molecular orbitals in liquid water are expected to be more extended,[42−44] and thus better overlap with each other, making the nonlocal decay processes more efficient than in a small finite-sized cluster. The more pronounced high kinetic energy shoulders in the experimental spectra relative to those in the theoretical spectra (see Figure 3) indicate that the above expectations are met.

The availability of nonlocal decay modes and proton transfer occurring after core ionization significantly diversify the manifold of the molecular species produced in X-ray irradiated liquid water. Our studies clearly show that unlike assumed so far in the literature, water dications H_2O^{2+} are by far not the only ionic species formed in water radiolysis. The two charges can separate through the PTM-Auger mechanism leading to OH^+ and H_3O^+ fragments. The ICD and ETMD processes

dx.doi.org/10.1021/ja5117588 | J. Am. Chem. Soc. 2014, 136, 18170−18176

occurring for the ground-state geometry give rise to two water cations, H_2O^+, which may act as extremely strong oxidants for molecules other than water.[45] Each H_2O^+ can also quickly lose a proton to the water environment[46,47] producing a highly reactive hydroxyl radical OH. Importantly, ETMD(3) predominantly creates two separate charges on molecules that are distinct from the core-ionized one, rendering this decay mode a significant and previously unconsidered mechanism of releasing oxidative stress. As seen from Figure 1, harmful OH radicals can also be generated directly via the PTM-ICD mechanism. These radicals are however transient species which recombine with protons to form cationic water molecules on yet to be determined time scales. Note that radiation damage can be induced also by primary and secondary electrons.[1,2] All these phenomena are important and should be taken into account when modeling X-ray induced damage of hydrated biomolecules.

CONCLUSIONS

Oxygen 1s Auger-electron spectra of liquid water, both H_2O and D_2O, have been simulated and analyzed in detail. Special emphasis has been given to reveal the origin of the high kinetic energy shoulder appearing in the autoionization spectra. We have demonstrated that together with ICD (both normal and proton-transfer mediated) and the PTM-Auger processes, also ETMD (both normal and proton-transfer mediated) substantially contributes to this spectral feature. A quantitative estimate for the relative importance of these three classes of processes has been provided.

Nonlocal ICD and ETMD processes not only contribute to the high kinetic energy part of the autoionization spectra but also to the central spectral region. Taken together, in the early time of the electronic decay, a substantial part of the total spectral intensity appears to be due to population of the final ICD and ETMD states (at least 40% in the model water pentamer considered). Ultrafast proton motion accompanying electronic relaxation identified through the experimental spectra, and corroborated theoretically,[26] further modifies this picture. Here, we have shown that proton transfer enhances the efficiency of the nonlocal processes considerably. Such nuclear dynamics has significant consequences for the radiation chemistry of water since the double charge formed in the electronic decay of X-ray irradiated liquid water will be distributed with rather high probability between different water monomers, rather than remaining localized on a single molecular unit.

The nonlocal electronic relaxation processes in hydrogen-bonded systems started to be extensively studied in recent years,[8−10,48,49] but the role played by nuclear dynamics was typically not considered yet. The PTM-CS mechanism seems to be a generic feature of hydrogen-bonded systems,[50,51] and thus, some of the previously studied systems, such as NH_3(aq),[7] should be revisited. Investigations along these lines are currently under way. It would be also useful to explore the effect of other degrees of freedom such as librations and structural diversity of liquid water on the calculated Auger spectrum. The first steps in this direction have been already made in this paper. We hope that Auger electron spectroscopy could potentially contribute to the present discussion on the structure of liquid water.

ASSOCIATED CONTENT

Supporting Information

Auger spectra and relative efficiencies of different relaxation processes computed for different water pentamers and a trimer. Justification of the choice of a single proton-transfer coordinate. This material is available free of charge via the Internet at http://pubs.acs.org.

AUTHOR INFORMATION

Corresponding Author

nikolai.kryzhevoi@pci.uni-heidelberg.de

Notes

The authors declare no competing financial interest.

ACKNOWLEDGMENTS

N.V.K., B.W., and L.S.C. gratefully acknowledge financial support by the DFG (project CE 10/45-2 and DFG Research Unit FOR 789). P.S. thanks to the support by Grant Agency of the Czech Republic, project number 13-34168S.

REFERENCES

(1) Mozumder, A.; Hatano, Y. *Charged particle and photon interactions with matter: chemical, physicochemical, and biological consequences with applications*; Marcel Dekker: New York, 2004.

(2) Garrett, B. C.; Dixon, D. A.; Camaioni, D. M.; Chipman, D. M.; Johnson, M. A.; Jonah, C. D.; Kimmel, G. A.; Miller, J. H.; Rescigno, T. N.; Rossky, P. J.; Xantheas, S. S.; Colson, S. D.; Laufer, A. H.; Ray, D.; Barbara, P. F.; Bartels, D. M.; Becker, K. H.; Bowen, H.; Bradforth, S. E.; Carmichael, I.; Coe, J. V.; Corrales, L. R.; Cowin, J. P.; Dupuis, M.; Eisenthal, K. B.; Franz, J. A.; Gutowski, M. S.; Jordan, K. D.; Kay, B. D.; LaVerne, J. A.; Lymar, S. V.; Madey, T. E.; McCurdy, C. W.; Meisel, D.; Mukamel, S.; Nilsson, A. R.; Orlando, T. M.; Petrik, N. G.; Pimblott, S. M.; Rustad, J. R.; Schenter, G. K.; Singer, S. J.; Tokmakoff, A.; Wang, L. S.; Wittig, C.; Zwier, T. S. *Chem. Rev.* **2005**, *105*, 355.

(3) Hirayama, R.; Ito, A.; Tomita, M.; Tsukada, T.; Yatagai, F.; Noguchi, M.; Matsumoto, Y.; Kase, Y.; Ando, K.; Okayasu, R.; Furusawa, Y. *Radiat. Res.* **2009**, *171*, 212.

(4) Cederbaum, L. S.; Zobeley, J.; Tarantelli, F. *Phys. Rev. Lett.* **1997**, *79*, 4778.

(5) Liegener, C.; Chen, R. J. *Chem. Phys.* **1988**, *88*, 2618.

(6) Öhrwall, G.; Fink, R. F.; Tchaplyguine, M.; Ojamäe, L.; Lundwall, M.; Marinho, R. R. T.; de Brito, A. N.; Sorensen, S. L.; Gisselbrecht, M.; Feifel, R.; Rander, T.; Lindblad, A.; Schulz, J.; Sæthre, L. J.; Mårtensson, N.; Svensson, S.; Björneholm, O. *J. Chem. Phys.* **2005**, *123*, 054310.

(7) Lindblad, A.; Bergersen, H.; Pokapanich, W.; Tchaplyguine, M.; Öhrwall, G.; Björneholm, O. *Phys. Chem. Chem. Phys.* **2009**, *11*, 1758.

(8) Kryzhevoi, N. V.; Cederbaum, L. S. *J. Phys. Chem. B* **2011**, *115*, 5441.

(9) Pokapanich, W.; Ottosson, N.; Svensson, S.; Öhrwall, G.; Winter, B.; Björneholm, O. *J. Phys. Chem. B* **2012**, *116*, 3.

(10) Kryzhevoi, N. V.; Cederbaum, L. S. *J. Phys. Chem. Lett.* **2012**, *3*, 2733.

(11) Zobeley, J.; Santra, R.; Cederbaum, L. S. *J. Chem. Phys.* **2001**, *115*, 5076.

(12) Pernpointner, M.; Kryzhevoi, N. V.; Urbaczek, S. *J. Chem. Phys.* **2008**, *129*, 024304.

(13) Averbukh, V.; Demekhin, P. V.; Kolorenc, P.; Scheit, S.; Stoychev, S. D.; Kuleff, A. I.; Chiang, Y.-C.; Gokhberg, K.; Kopelke, S.; Sisourat, N.; Cederbaum, L. S. *J. Electron Spectrosc. Relat. Phenom.* **2011**, *183*, 36.

(14) Hergenhahn, U. *Int. J. Radiat. Biol.* **2012**, *88*, 871.

(15) Sakai, K.; Stoychev, S.; Ouchi, T.; Higuchi, I.; Schoeffler, M.; Mazza, T.; Fukuzawa, H.; Nagaya, K.; Yao, M.; Tamenori, Y.; Kuleff, A. I.; Saito, N.; Ueda, K. *Phys. Rev. Lett.* **2011**, *106*, 033401.

(16) Förstel, M.; Mucke, M.; Arion, T.; Bradshaw, A. M.; Hergenhahn, U. *Phys. Rev. Lett.* **2011**, *106*, 033402.
(17) Morin, P.; Nenner, I. *Phys. Rev. Lett.* **1986**, *56*, 1913.
(18) Pahl, E.; Cederbaum, L. S.; Meyer, H. D.; Tarantelli, F. *Phys. Rev. Lett.* **1998**, *80*, 1865.
(19) Hjelte, I.; Piancastelli, M. N.; Fink, R. F.; Björneholm, O.; Bässler, M.; Feifel, R.; Giertz, A.; Wang, H.; Wiesner, K.; Ausmees, A.; Miron, C.; Sorensen, S. L.; Svensson, S. *Chem. Phys. Lett.* **2001**, *334*, 151.
(20) Brena, B.; Nordlund, D.; Odelius, M.; Ogasawara, H.; Nilsson, A.; Pettersson, L. G. M. *Phys. Rev. Lett.* **2004**, *93*, 148302.
(21) Odelius, M.; Ogasawara, H.; Nordlund, D.; Fuchs, O.; Weinhardt, L.; Maier, F.; Umbach, E.; Heske, C.; Zubavichus, Y.; Grunze, M.; Denlinger, J. D.; Pettersson, L. G. M.; Nilsson, A. *Phys. Rev. Lett.* **2005**, *94*, 227401.
(22) Fuchs, O.; Zharnikov, M.; Weinhardt, L.; Blum, M.; Weigand, M.; Zubavichus, Y.; Baer, M.; Maier, F.; Denlinger, J. D.; Heske, C.; Grunze, M.; Umbach, E. *Phys. Rev. Lett.* **2008**, *100*, 027801.
(23) Tokushima, T.; Harada, Y.; Takahashi, O.; Senba, Y.; Ohashi, H.; Pettersson, L. G. M.; Nilsson, A.; Shin, S. *Chem. Phys. Lett.* **2008**, *460*, 387.
(24) Ljungberg, M. P.; Nilsson, A.; Pettersson, L. G. M. *Phys. Rev. B* **2010**, *82*, 245115.
(25) Nilsson, A.; Tokushima, T.; Horikawa, Y.; Harada, Y.; Ljungberg, M. P.; Shin, S.; Pettersson, L. G. M. *J. Electron Spectrosc. Relat. Phenom.* **2013**, *188*, 84.
(26) Thürmer, S.; Ončák, M.; Ottosson, N.; Seidel, R.; Hergenhahn, U.; Bradforth, S. E.; Slavíček, P.; Winter, B. *Nat. Chem.* **2013**, *5*, 590.
(27) Winter, B.; Faubel, M. *Chem. Rev.* **2006**, *106*, 1176.
(28) Woon, D.; Dunning, T. *J. Chem. Phys.* **1995**, *103*, 4572.
(29) Kendall, R.; Dunning, T.; Harrison, R. *J. Chem. Phys.* **1992**, *96*, 6796.
(30) Werner, H.-J.; Knowles, P. J.; Knizia, G.; Manby, F. R.; Schütz, M.; and et al. *MOLPRO*, version 2010.1, a package of ab initio programs; University College Cardiff Consultants Limited: Cardiff, Wales, U.K., 2010.
(31) Schirmer, J.; Barth, A. *Z. Phys. A: Hadrons Nucl.* **1984**, *317*, 267.
(32) Velkov, Y.; Miteva, T.; Sisourat, N.; Schirmer, J. *J. Chem. Phys.* **2011**, *135*, 154113.
(33) Kuchle, W.; Dolg, M.; Stoll, H.; Preuss, H. *Mol. Phys.* **1991**, *74*, 1245.
(34) Tarantelli, F.; Sgamellotti, A.; Cederbaum, L. S. *J. Chem. Phys.* **1991**, *94*, 523.
(35) Skinner, L. B.; Huang, C.; Schlesinger, D.; Pettersson, L. G. M.; Nilsson, A.; Benmore, Ch. J. *J. Chem. Phys.* **2013**, *138*, 074506.
(36) Wernet, P.; Nordlund, D.; Bergmann, U.; Cavalleri, M.; Odelius, M.; Ogasawara, H.; Naslund, L.-Å.; Hirsch, T. K.; Ojamäe, L.; Glatzel, P.; Pettersson, L. G. M.; Nilsson, A. *Science* **2004**, *304*, 995.
(37) Smith, J. D.; Cappa, C. D.; Wilson, K. R.; Messer, B. M.; Cohen, R. C.; Saykally, R. J. *Science* **2004**, *306*, 851.
(38) Huang, C.; Wikfeldt, K. T.; Tokushima, T.; Nordlund, D.; Harada, Y.; Bergmann, U.; Niebuhr, M.; Weiss, T. M.; Horikawa, Y.; Leetmaa, M.; Ljungberg, M. P.; Takahashi, O.; Lenz, A.; Ojamäe, L.; Lyubartsev, A. P.; Shin, S.; Pettersson, L. G. M.; Nilsson, A. *Proc. Natl. Acad. Sci. U. S. A.* **2009**, *106*, 15214.
(39) Clark, G. N. I.; Cappa, C. D.; Smith, J. D.; Saykally, R. J.; Head-Gordon, T. *Mol. Phys.* **2010**, *108*, 1415.
(40) Henchman, R. H.; Cockram, S. *J. Faraday Discuss.* **2013**, *167*, 529.
(41) Kuehne, T. D.; Khaliullin, R. Z. *Nat. Commun.* **2013**, *4*, 1450.
(42) Prendergast, D.; Grossman, J. C.; Galli, G. *J. Chem. Phys.* **2005**, *123*, 014501.
(43) Cabral do Couto, P.; Estácio, S. G.; Costa Cabral, B. J. *J. Chem. Phys.* **2005**, *123*, 054510.
(44) Nordlund, D.; Ogasawara, H.; Bluhm, H.; Takahashi, O.; Odelius, M.; Nagasono, M.; Pettersson, L. G. M.; Nilsson, A. *Phys. Rev. Lett.* **2007**, *99*, 217406.
(45) Ma, J.; Schmidhammer, U.; Pernot, P.; Mostafavi, M. *J. Phys. Chem. Lett.* **2013**, *5*, 258.
(46) Han, P.; Bartels, D. M. *J. Phys. Chem.* **1990**, *94*, 5824.
(47) Li, J.; Nie, Z.; Zheng, Y. Y.; Dong, S.; Loh, Z.-H. *J. Phys. Chem. Lett.* **2013**, *4*, 3698.
(48) Schwartz, C. P.; Fatehi, S.; Saykally, R. J.; Prendergast, D. *Phys. Rev. Lett.* **2010**, *105*, 198102.
(49) Aziz, E. F.; Ottosson, N.; Faubel, M.; Hertel, I. V.; Winter, B. *Nature* **2008**, *455*, 89.
(50) Thürmer, S.; Unger, I.; Slavíček, P.; Winter, B. *J. Phys. Chem. C* **2013**, *117*, 22268.
(51) Unger, I.; Thürmer, S.; Hollas, D.; Aziz, E. F., Winter, B.; Slavíček, P. *J. Phys. Chem. C*, **2014**; doi: 10.1021/jp504707h.